Nat Hazards (2009) 51:183–205
DOI 10.1007/s11069-009-9381-4

ORIGINAL PAPER

A surge response function approach to coastal hazard assessment. Part 2: Quantification of spatial attributes of response functions

Jennifer L. Irish · Donald T. Resio · Mary A. Cialone

Received: 30 July 2008 / Accepted: 4 March 2009 / Published online: 20 March 2009

Abstract In response to the 2004 and 2005 hurricane seasons, surge risk assessment approaches have been re-evaluated to develop more rapid, reliable methods for predicting the risk associated with extreme hurricanes. Here, the development of dimensionless surge response functions relating surge to hurricane meteorological parameters is presented. Such response functions present an opportunity to maximize surge data usage and to improve statistical estimates of surge probability by providing a means for defining continuous probability density functions. A numerical modeling investigation was carried out for the Texas, USA coastline to develop physical scaling laws relating storm surge response with hurricane parameters including storm size, intensity, and track. It will be shown that these scaling laws successfully estimate the surge response at any arbitrary location for any arbitrary storm track within the study region. Such a prediction methodology has the potential to decrease numerical computation requirements by 75% for hurricane risk assessment studies.

Keywords Storm surge · Coastal flooding · Coastal hazards · Tropical cyclones · Hurricanes · Risk assessment

List of symbols

ADCIRC	ADvanced CIRCulation model, a finite-element long-wave numerical model
B	Hurricane pressure profile peakedness parameter (Holland 1980)
c_p	Hurricane central barometric pressure, a measure of hurricane intensity
JPM	Joint probability method
JPM-OS	Joint probability method with optimal sampling
m_x	Location-dependent constant relating hurricane surge to intensity

J. L. Irish (✉)
Coastal and Ocean Engineering Division, Zachry Department of Civil Engineering,
Texas A&M University, College Station, TX 77843-3136, USA
e-mail: jirish@civil.tamu.edu

D. T. Resio · M. A. Cialone
Coastal and Hydraulics Laboratory, U.S. Army Engineer Research and Development Center,
Vicksburg, MS 39186, USA

R_{p}	Hurricane pressure radius, a measure of hurricane size
R_{thresh}	Threshold hurricane pressure radius for small storms
R'	Dimensionless hurricane pressure radius
X	Distance alongshore
x'	Preliminary dimensionless alongshore distance
$x_2{}'$	Dimensionless alongshore distance
x_{o}	Distance alongshore, x, at the eye location at landfall
$x_{\zeta_{\mathrm{peak}}}$	Distance alongshore, x, at the location of peak alongshore surge
(x, y)	Geographic position
$(x_{\mathrm{o}}, y_{\mathrm{o}})$	Geographic position of storm eye at landfall
Δp	Central pressure deficit
γ	Specific weight of water
λ	Constant relating location of peak alongshore surge to storm size
Φ	Dimensionless surge response surface
ϕ_{km}	Dimensional surge response function
ζ	Maximum hurricane surge at a given location (x, y)
ζ'	Dimensionless surge
ζ_{peak}	Peak alongshore surge
ζ_{sim}	Numerically simulated maximum hurricane surge at a given location (x, y)
ζ_{Φ}	Predicted maximum hurricanes surge at a given location (x, y) using surge response function

1 Introduction

Following the hurricane seasons of 2004 and 2005, the reliability of conventional methodologies for assessing flooding risk for extreme hurricane events has been brought into question. Resio et al. (2009) presented a comprehensive background and history on extreme-value statistics for coastal flooding and discussed their shortcomings when used to assess flooding. In order to overcome many of the shortcomings associated with existing statistical approaches, Resio et al. (2009) presented a new method for determining coastal flooding risk based upon the joint probability method (JPM) with optimal sampling (JPM-OS). This new approach allows for a more reliable estimate of extreme flood level risk, a better quantification of the uncertainty associated with these risk estimates, and a more efficient use of numerical analysis and historical observations. These benefits of the JPM-OS are derived from the proposed surge response function approach which suggests that a continuous surface for maximum surge (ζ) at a particular geographic location (x, y) for a given storm track angle with respect to the coastline k, storm forward speed m, and eye location at landfall $(x_{\mathrm{o}}, y_{\mathrm{o}})$ is given by:

$$\zeta(x, y) = \phi_{km}\left([x_{\mathrm{o}}, y_{\mathrm{o}}], [c_p, R_{\mathrm{p}}], [x, y]\right), \tag{1}$$

where ϕ_{km} is the dimensional surge response function for track angle k and forward speed m, c_p is the hurricane central pressure, and R_{p} is the hurricane pressure radius. The above definition for surge response allows for the development of a continuous, as opposed to discretized, probability density function from which flooding risk due to extreme coastal storms can be more accurately defined. This surge response surface approach also presents a means for optimally sampling the storm population in order to minimize computational

requirements for storm surge modeling studies for risk assessment, and for gleaning more information from historical observations.

The motivation for the investigation presented here is to show that surge response functions demonstrate continuous behavior with respect to both meteorological conditions and changes in coastal landscape, and that these surge response functions can be estimated based on a limited and discrete set of surge values.

The following sections first present an analysis of numerical surge simulation results for a regional coastline on the Gulf of Mexico to produce continuous surge response surfaces, then present a parameterization of the numerical results for use in estimating surge response functions from limited surge data.

2 Surge response surface development by numerical simulation

In order to verify the concept and validity of the surge response function approach, a numerical investigation was conducted for the northwestern Gulf of Mexico, along the coast of Texas. Below, the numerical modeling methodology and simulated storm surge results are discussed.

2.1 Numerical simulation methodology

Storm surges along the Texas coastline were computed using the finite-element long-wave numerical model ADCIRC (Westerink et al. 1992, 2007). The ADCIRC model domain included the entire Gulf of Mexico water body and the North Atlantic basin to 60°W longitude, and the domain highly resolved the entire northern Gulf of Mexico nearshore and inland bay system particularly along the Texas coast (Fig. 1). This numerical domain

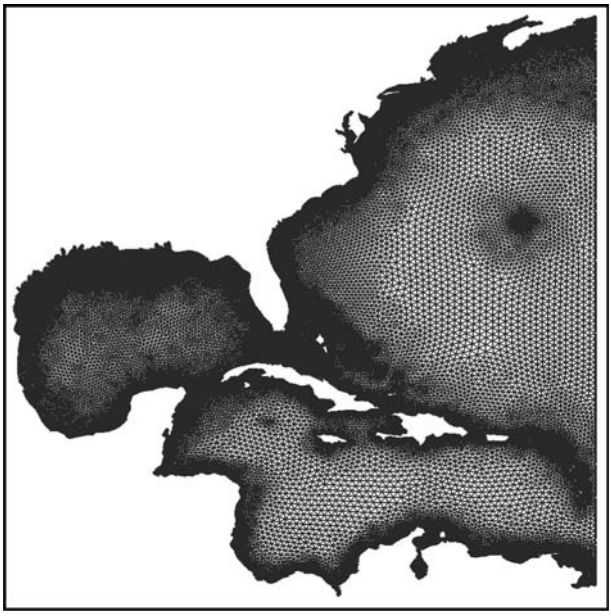

Fig. 1 ADCIRC computational domain

and associated calibration inputs were rigorously verified for surge simulation demonstrating accuracy well within 30 cm for most locations within inland bays and along the open coast throughout the northern Gulf of Mexico (U.S. Army Corps of Engineers 2006a, b). Storm surge modeled within ADCIRC for this investigation was forced with meteorological inputs for wind and barometric pressure fields. Tidal forcing and ocean wave setup, both of which can add to storm surge, are beyond the scope of this paper. Astronomical tide can typically be considered as a linear addition to surge level in many applications, and added surge level by wave-induced setup, which typically contributes much less to total flood level than wind-induced surge for high surge events, is anticipated to scale in a similar manner as the wind-induced surge considered here.

In order to develop surge response surfaces at multiple locations within a real coastal system, a parametric representation of tropical cyclone meteorology was adopted. Seeking a surge response surface in the form of Eq. 1, central pressure (c_p), storm size (R_p), storm forward speed (v_f), and peakedness B (Holland 1980), in conjunction with an assumed background pressure field, were used as input to a coupled hurricane vortex—planetary boundary layer (PBL) model (Thompson and Cardone 1996) to estimate sustained near-surface winds throughout the storm.

Hurricanes impacting the Texas coast may be divided into three classes: (1) those entering the Gulf of Mexico between Florida and Cuba which follow a northwesterly path, (2) those entering the Gulf of Mexico between Cuba and the Yucatan peninsula which follow a northwesterly path, and (3) those entering the Gulf of Mexico after passing over the Yucatan peninsula, or those forming initially within the Gulf of Mexico, which follow a north northeasterly path. This investigation focuses on four hurricanes of the first class, where the tracks are spaced 30 km apart. The selected hurricane tracks parallel each other and have track angles at landfall, with respect to the coastline, of less than 17° (Fig. 2). While storm track angle with respect to the coastline (Niedoroda et al. in review) and storm forward speed can alter maximum surge at the coast, in this investigation peak surge response to these parameters is not considered in order to simplify the analysis. Storm forward speed for all simulations was 5.7 m/s and represents a typical forward speed for hurricanes in the Gulf of Mexico (Dorst 2007). We acknowledge, however, that in more northern locations (such as the mid-Atlantic and Northeast coasts of the U.S.), the historical record shows average hurricane forward speeds to be greater than 5.7 m/s (Dorst

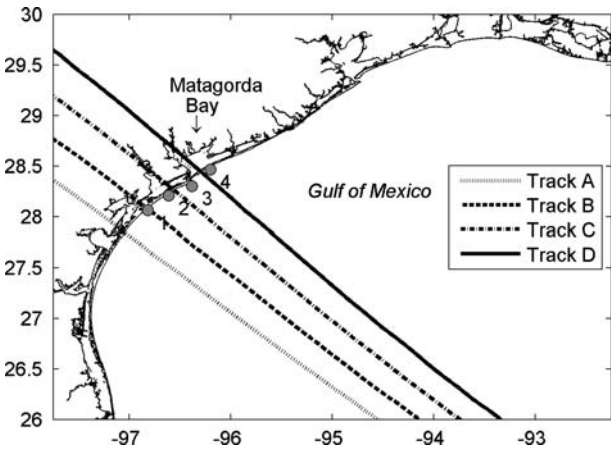

Fig. 2 Location map showing hurricane tracks considered in this analysis and sample output locations

2007). By holding track angle and hurricane forward speed constant, specific application of the results presented here will be limited in applicability to the track angles and storm forward speed considered here.

Sensitivity to variation in storm peakedness (Holland B), from 0.9 to 1.9, was evaluated with ADCIRC and demonstrated only small changes in peak surge, on the order of 15%. As such, surge variation with storm peakedness was not considered further in this investigation. Instead, Holland B for all simulations was held constant at 1.27 until the last 50 km before landfall at which point Holland B was decreased linearly to a value of 1.00 at landfall. These values for Holland B represent typical hurricane conditions in the Gulf of Mexico.

Multiple parameterized storms for simulation were created for each track by varying hurricane intensity (c_p) from 900 to 960 mb and size (R_p) from 11 to 65 km. Surges for a minimum of 17 storm intensity and storm size combinations were simulated for each track, with additional simulations added as needed to verify trends in surge response surfaces. In all, 75 numerical storm surge simulations were executed and evaluated.

2.2 Impact of hurricane intensity and size on surge magnitude and extent

For each simulation, modeled hurricane surge along the open coast was analyzed to determine the impact of both hurricane intensity and hurricane size on surge magnitude and on the distribution of surge along the coast. Figures 3 and 4 show the alongshore

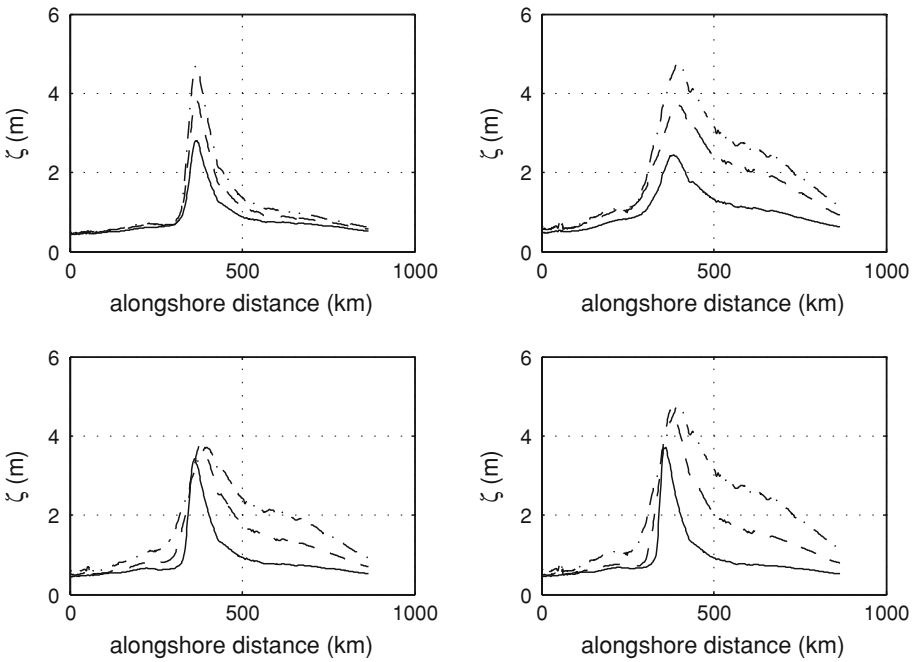

Fig. 3 Numerically simulated surge variation alongshore for selected storms on Track A. Top panes show surge variation with intensity [c_p = 960 mb (*solid*), 930 mb (*dashed*), and 900 mb (*dash-dot*)] when size R_p = 20.4 km (*top left*) and 65.9 km (*top right*); bottom panes show surge variation with size [R_p around 15 km (*solid*), 30 km (*dashed*), and 65 km (*dash-dot*)] when intensity c_p = 930 mb (*bottom left*) and 900 mb (*bottom right*)

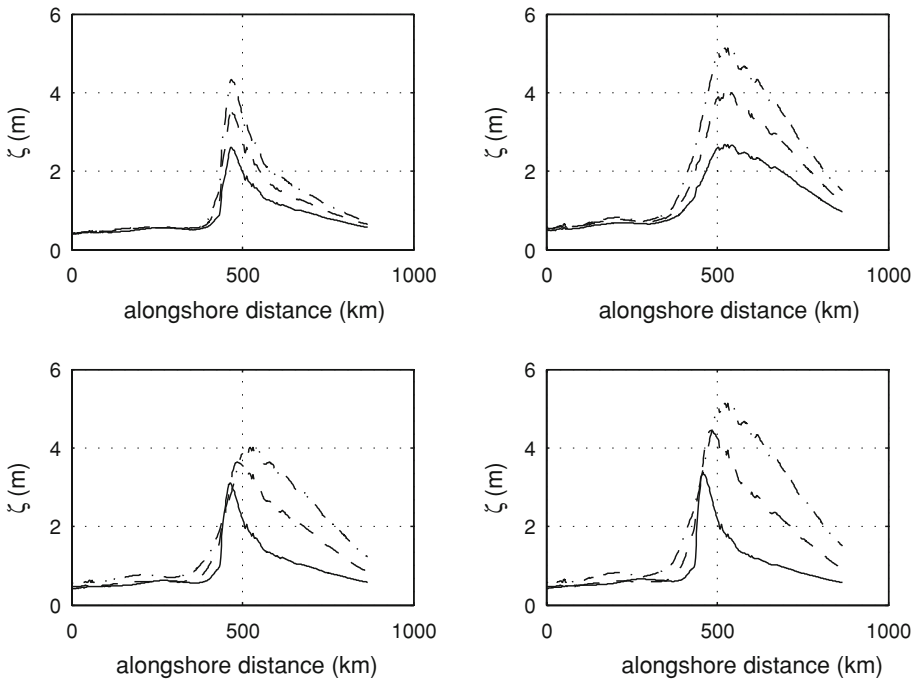

Fig. 4 Numerically simulated surge variation alongshore for selected storms on Track D. Top panes show surge variation with intensity [c_p = 960 mb (*solid*), 930 mb (*dashed*), and 900 mb (*dash-dot*)] when size R_p = 20.4 km (*top left*) and 65.9 km (*top right*); bottom panes show surge variation with size [R_p around 15 km (*solid*), 30 km (*dashed*), and 65 km (*dash-dot*)] when intensity cp = 930 mb (*bottom left*) and 900 mb (*bottom right*)

distribution of hurricane surge for selected simulations on Tracks A and D, respectively. The top panes in both figures, where hurricane size is held constant, demonstrate that the peak alongshore surge uniformly increases with increasing hurricane intensity. For small to moderately sized storms (top left panes), peak alongshore surge increases about 30 cm per 10 mb of intensification. Large storms result in a relatively large rate of increase of peak surge; for large storms (top right panes), peak alongshore surge increases about 40 cm per 10 mb. The top panes of Figs. 3 and 4 also show that the alongshore distribution from one intensity to the other is similar in shape and generally scales with peak alongshore surge.

The bottom panes of Figs. 3 and 4, where hurricane intensity is held constant, show that as hurricane size increases hurricane surge tends to increase as well (Irish et al. 2008). As hurricane size increases from small (10–15 km) to moderate (20–30 km), the largest relative rise in peak alongshore surge is observed on all Tracks, between 0.5 and 1.0 m per 10 km increase in R_p. As storm size continues to increase, the simulation results indicate that the relative rise in peak alongshore surge is milder, increasing up to 20 cm per 10 km. Unlike with intensity, the relative location of landfall appears to govern the degree to which surge increases with hurricane size. For example, along Track D peak alongshore surge gradually rises for all storm sizes. In contrast, along Track A peak alongshore surge rises initially with increasing size then appears to stabilize. This is most probably related to the relative size of the hurricane with respect to the continental shelf width. The cross-shore shelf width along and to the north of Track A is narrower than the cross-shore shelf width along and to the northeast of Track D. Therefore, for Track D the relatively large

shallow shelf region provides a larger area over which surge may be generated during larger storms.

From a regional risk-assessment perspective, the alongshore extent of elevated surge levels is important. Figures 3 and 4 demonstrate that for larger hurricanes the extent of high surge levels increases substantially with increasing size for all tracks and all storm intensities. For example, the alongshore extent of surge levels over 2 m increases by 20–100% per 10 km increase in R_p. This elevated surge along the coast is most dramatic to the right of hurricane landfall, as expected.

2.3 Simulated surge response surfaces

For each of the four tracks, surge response surfaces by track were developed at four locations at 10-m depth along the open coast (Fig. 5) based on hurricane meteorological characteristics taken ~165 km from landfall. In all cases, surge for a given storm track at a particular location varies relatively smoothly with changes in both hurricane intensity and hurricane size. In the vicinity of the landfall location and point of peak alongshore surge

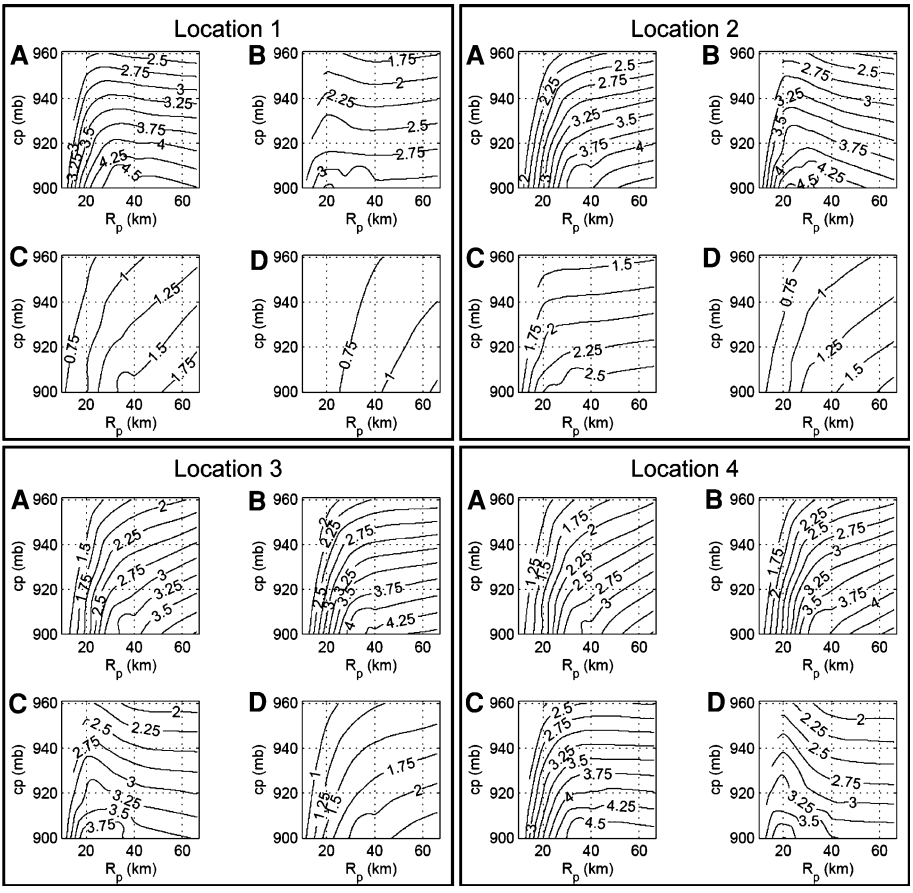

Fig. 5 Numerically simulated surge response surfaces at locations 1 through 4 (see Fig. 2) for all storms on Tracks A through D. Peak surge contours shown at 0.25-m intervals

(Fig. 5; Locations 1 and 2 for Track B, Location 3 for Track C, and Location 4 for Track D), the surge response surfaces have somewhat complex characteristics. In particular, the influence of storm size yields a positive bulge, or ridge, in the surge response surface for small storms for locations close to the landfall location. Further to the right of the landfall location, this bulge becomes relatively less peaked (Fig. 5; e.g., Location 1 for Track A) as the influence of storm size more broadly impacts the response surface at a distance on the order of one times the storm radius from the landfall location. This influence becomes less pronounced at a distance on the order of 1.5 times the storm radius to the right of the landfall location (Fig. 5; e.g., Location 2 for Track A and Location 3 for Track B).

Beyond this distance, the surge response surfaces vary more gradually with both storm intensity and size. Well to the right of the landfall location and point of peak alongshore surge (Fig. 5; e.g., Locations 3 and 4 for Track A and Location 4 for Track B), the surge response surfaces exhibit monotonically increasing surge values with both increasing storm size and increasing storm intensity. Furthermore, at these locations surge varies almost linearly with storm intensity for a given storm size, thus indicating that a small sample of storms can adequately define these surge response surfaces (Fig. 6). Locations to the left of the storm track, away from the landfall location, also exhibit uniformly increasing surge with both increasing storm size and intensity (Fig. 5; e.g., Locations 1, 2, and 3 for Track D).

When considering the surge response surface variation with track for a given alongshore location, storm size dictates which track yields a more severe surge level. At an alongshore location just to the right of Track B (Location 2 on Fig. 5), Track B's surge response surface yields the largest surge for all small to moderately sized storms. However, the surge response surface for Track A at this same location, which tracked about 50 km to the left of Location 2, demonstrates larger surges than Track B when storm size is very large.

The characteristic shapes described above for these numerically simulated surge response surfaces suggest that these surfaces may be reasonably described by a few storm parameters. The following section describes an approach for parameterizing the surge

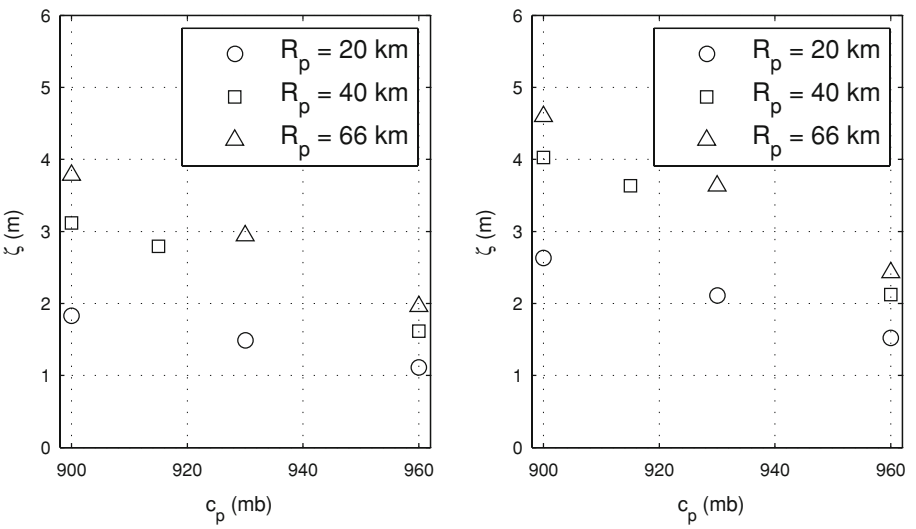

Fig. 6 Central pressure versus numerically simulated surge at Location 4 (see Fig. 2) for selected storms on Tracks A (*left pane*) and B (*right pane*)

response surfaces as a means to optimize numerical simulations and subsequent data analysis.

3 Surge response function estimation

Numerical storm surge simulations are highly computationally intensive with one individual storm simulation requiring more than 1,000 h of CPU time (based on simulations made on a Cray XT3 and on a Linux cluster). In addition, the physics solved within the surge model itself becomes more and more complex as effects due to waves, inland runoff, and morphodynamic change are dynamically coupled with the hydrodynamic model in order to achieve a higher degree of accuracy in the simulated surge estimate. Compounding the computational time requirements is the necessity for comprehensive coverage of all storm parameters to effectively implement traditional JPM-type extreme value statistics methods. Typically, such studies require an array of storm track orientations with a sequence of tracks spaced about 25 km apart per orientation. Thus, from a practical standpoint, the number of individual storm surge simulations required for a coastal flood risk-assessment study must be minimized.

In this section, physical scaling laws are introduced which cast the surge response into a dimensionless form in a way that lends itself to better interpolation of surge response for storm scenarios not explicitly represented by the simulated storm set.

3.1 Physical scaling laws for hurricane surge response

At a given alongshore location for a given storm track, the numerically simulated results suggest that storm surge at a location of interest scales with storm intensity and size and with proximity to the eye location at landfall. Using the numerically simulated surge values, a dimensionless surge response function was developed. First, an analysis of simulated surges demonstrated a strong correlation, with R^2 of 0.85 for all tracks, between storm size and distance between the location of peak alongshore surge and the eye location at landfall (Fig. 7). For all tracks, the numerical results also indicate that this distance between peak surge $\left(\zeta_{\text{peak}}\right)$ and storm eye can, to first order, be described by a linear function of storm size with slope, λ:

$$x_{\zeta_{\text{peak}}} - x_{\text{o}} \cong \lambda R_{\text{p}}, \tag{2}$$

where x is taken as distance measured along an axis running alongshore (Fig. 2) such that $x_{\zeta_{\text{peak}}}$ is the distance alongshore to the location of peak alongshore surge and x_{o} is the distance alongshore to the eye location at landfall. This relationship may also be used to determine the relative distance between an alongshore location of interest and the location of peak surge $\left(x - x_{\zeta_{\text{peak}}}\right)$. By performing a linear regression on the numerically simulated surges, the slope for all storms on all tracks was determined to be $\lambda = 0.87$. Average percent error for the numerically simulated distance between eye location at landfall and peak alongshore surge with respect to that distance predicted with Eq. 2 is better than 17% (calculated as the difference between the simulated and predicted values normalized by the simulated value). It should be noted, however, that the error in the predicted estimate can readily be accounted for in the uncertainty term in the JPM-OS approach to extreme-value statistics (Resio et al. 2009).

The numerically simulated surges (see Figs. 3, 4) suggest that the alongshore distribution of surge, when normalized by ζ_{peak}, decreases consistently with distance from $x_{\zeta_{\text{peak}}}$,

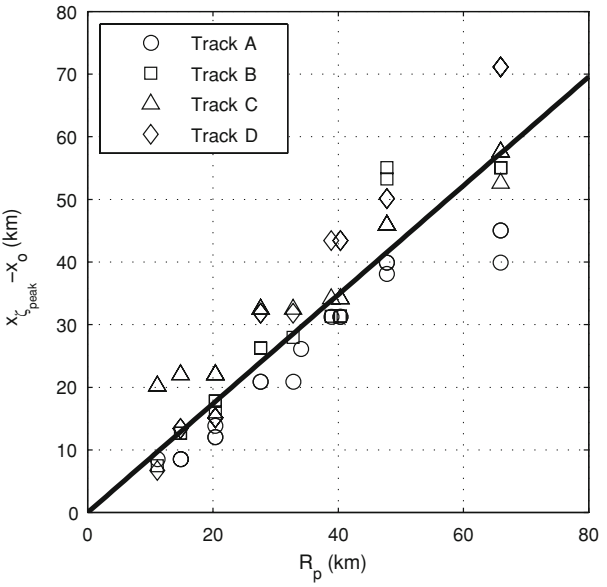

Fig. 7 Numerically simulated alongshore location of peak surge versus storm size for all simulated storms

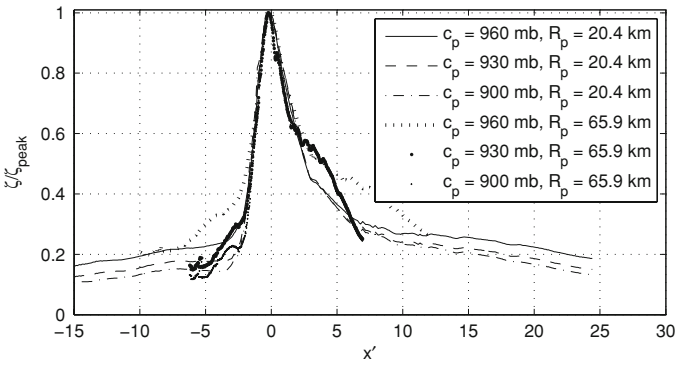

Fig. 8 Numerically simulated dimensionless alongshore surge distribution for selected storms on Track A

when alongshore distance is normalized by storm size (Fig. 8). For extreme-value statistics, the surge levels of interest are those at or near the peak surge value, and the normalized surge distribution for all simulated storms closely align when surge levels are >60% of the peak alongshore surge. Thus, a dimensionless alongshore dimension (x') is introduced:

$$x' = \frac{(x - x_o)}{R_p} - \lambda. \tag{3}$$

In order to develop a dimensionless surge parameter which is independent of surge at other locations e.g., (ζ_{peak}), a dimensionless surge (ζ') as a function of ζ at the location of interest (x) and c_p is defined as:

$$\zeta' = \frac{\gamma\zeta}{\Delta p} + m_x \Delta p, \tag{4}$$

where Δp is the pressure differential between the far-field barometric pressure and c_p, γ is specific weight of water, and m_x is a location-dependent constant determined by linear regression. From a physical perspective, the first term in Eq. 4 represents to first order the momentum balance for surge generation, where Δp can be considered proportional to wind speed squared. The second term in Eq. 4 can be considered representative of additional wind drag effects. Based on the numerical simulations and Texas locations considered here, values for m_x vary from 0.007 to 0.012 mb^{-1} (for Δp in mb).

Figure 9 shows the dimensionless surge response function for Locations 1 through 4 based on the dimensionless parameters ζ' and x' as defined by Eqs. 3 and 4. This figure shows that these two dimensionless parameters largely describe the surge response, by collapsing the dimensionless surge (ζ') into a single surge response function. Consider Location 1, which is located at the landfall location of Track B and well to the southwest of Tracks B and C and about 25 km to the northeast of Track A. At this location, all storms with $x' < 0$ follow the same response distribution while all storms at $x' = 0$ collapse to a single value of ζ'. Location 2, located just southwest of Track C and centered among the other tracks, similarly exhibits a single alongshore response distribution when $x' < 0$. Additionally, ζ' at Location 2 follows the same alongshore distribution for all storms when $x' > 0$. However, at Location 2 some scatter is evident near the peak of the distribution, around $x' = 0$.

At Location 3, however, there are a few notable exceptions which do not follow a single alongshore distribution. These storms, marked by circles in Fig. 9, are those storms which are relatively small and make landfall just southwest of Location 3 (Track C). These storms further coincide with the bulge, or ridge, observed in the surge response surface for Track C (Fig. 5, bottom left pane). From the simulated data, it is evident that there is a secondary effect related to the relative landfall proximity of small storms. By inspection of the simulated data (see location of ridge features in Fig. 5), a natural size threshold (R_{thres}) for the Texas location considered here for defining "small storms" is $R_p < 25$ km. In order to quantify this secondary effect, all storms with $R_p < R_{\text{thres}}$ and $-\lambda < x' < \lambda$ were identified (circled storms on Fig. 5) and compared to the dimensionless distributions presented in Fig. 5. In order to collapse this class of storms into the existing surge response function, a revised dimensionless alongshore dimension (x_2') was defined:

$$x_2' = x' - F(1 - R')H(1 - R'), \tag{5}$$

where $R' = R_p/R_{\text{thres}}$ is the dimensionless hurricane size, $H(1 - R')$ is the Heaviside function ($H(x) = 1$ for $x \geq 0$ and $= 0$ for $x < 0$), and $F(1 - R')$ is a ramp function defined as:

$$F(1-R') = \begin{array}{ll} a_1(1-R') + b_1, & -\lambda \leq x' \leq 0, \\ a_2(1-R') + b_2, & 0 < x' \leq \lambda \\ 0, & \lambda < |x'|. \end{array}, \tag{6}$$

The coefficients a and b of this ramp function were determined by linear regression between the quantity $(1 - R')$ and the difference between the initial value of x' and the corresponding value of x' on the existing surge response function, where ζ' is kept constant (Fig. 9). In Eq. 6, the division into three ranges can be seen on Fig. 9. Small storms making landfall just to the southwest of the location (circles with $x' < 0$ in Fig. 9, bottom panes) are adjusted using the $a_1 - b_1$ ramp function, while small storms making landfall

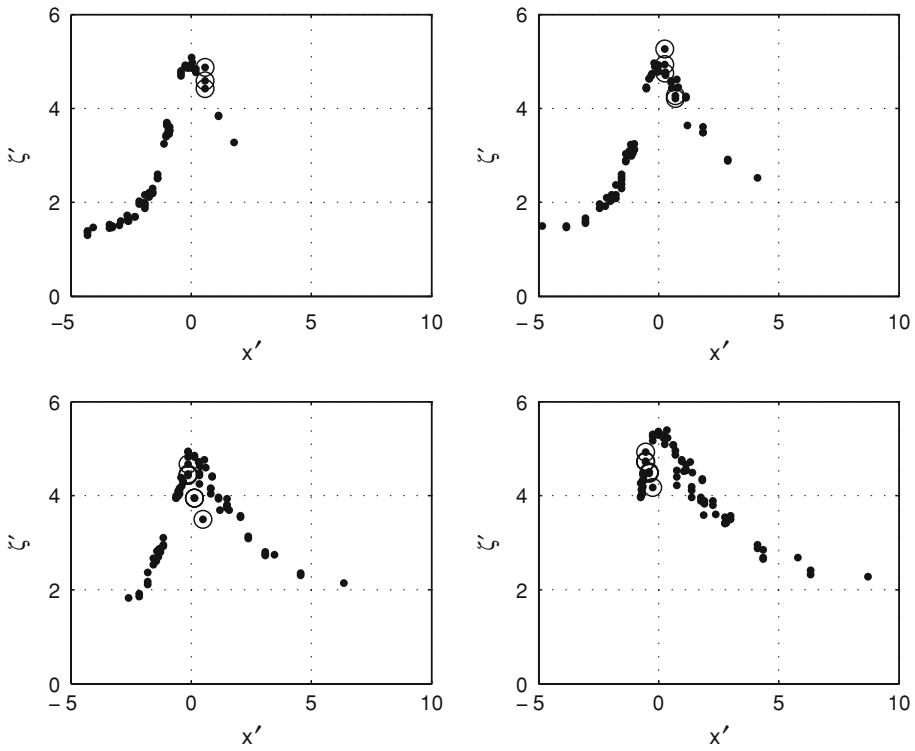

Fig. 9 Preliminary dimensionless surge response functions using all simulated storms on all four tracks for Locations 1 (*top left*), 2 (*top right*), 3 (*bottom left*), and 4 (*bottom right*). Circled storms are those with $R_p < 25$ km and $-\lambda < x' < \lambda$

just to the northeast of the location (circles with $x' > 0$ in Fig. 9, top panes) are adjusted using the $a_2 - b_2$ ramp function. Based on the full suite of numerical simulations, the coefficient values for this stretch of the Texas coast were determined to be $a_1 = -1.04$, $b_1 = 0.16$, $a_2 = 3.29$, and $b_2 = -0.67$.

Figure 10 shows the revised dimensionless relationships defined by ζ' versus x_2'. As this figure shows, the surge response is almost completely described by this new function, where the anomalous small storms now align with the rest of the distribution. While there is some scatter evident when $x' > 0$, the general trend is made clear. This small amount of scatter is most likely attributed to the combined effect of hurricane size and regional geometry, namely continental shelf width and orientation, and shoreline orientation.

It is worth noting that from location to location within the study area, the response function shape and magnitude along the open coast varies slowly. This indicates that in areas with slowly varying geographic features, interpolation of surge between locations for which surge data are available (e.g., water level measurement locations) to a reasonable degree of accuracy should be possible. It is important, however, to recognize that the response function shape and magnitude will likely vary more substantially within coastal embayments, so care should be given when interpolating between locations if using historical observations collected within coastal bays. Conversely, a response function developed from historical data at any given location (even within a coastal embayment)

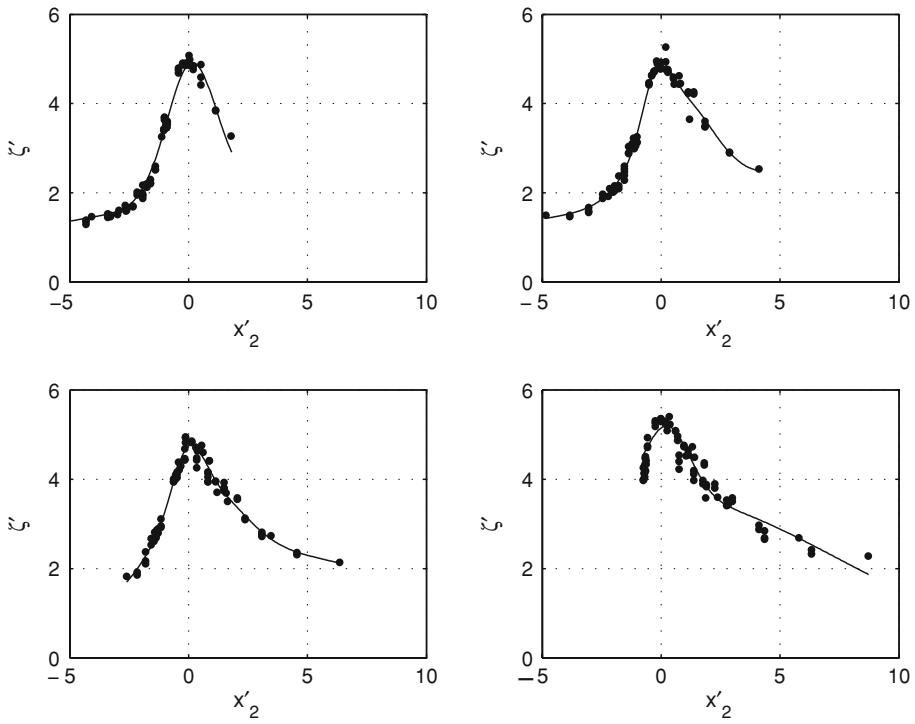

Fig. 10 Dimensionless surge response functions using modified dimensionless alongshore parameter and using all simulated storms on all four tracks for Locations 1 (*top left*), 2 (*top right*), 3 (*bottom left*), and 4 (*bottom right*). Solid line shows 3-term Gaussian fit to data

can be expected to perform well for estimating the surge response at that location for any hurricane event.

Equations 4 through 6 provide a means for predicting surge response functions from limited data, and as will be shown below, these relationships effectively predict surge response for storms not explicitly represented by numerical simulations.

3.2 Response function prediction from limited data

In this section, we examine the use and accuracy of dimensionless surge response functions developed from limited surge data sets to predict surge response over a range of conditions in order to optimize numerical simulations and to maximize the knowledge gained from field measurements. Specifically, we will consider spatial data sets limited by track spacing and range of c_p and data sets limited by spatial coverage. The dimensionless surge response functions (Φ) developed from the 75 numerically simulated surges appear to be generally described by a Gaussian distribution in the form:

$$\Phi(x_2') = a_1 e^{-\left(\frac{x_2'-b_1}{c_1}\right)^2} + a_2 e^{-\left(\frac{x_2'-b_2}{c_2}\right)^2} + a_3 e^{-\left(\frac{x_2'-b_3}{c_3}\right)^2}, \quad (7)$$

where a_1, b_1, c_1, a_2, b_2, c_2, a_3, b_3, and c_3 are curve-fitting coefficients determined by least-squares regression. As seen in Fig. 10, the Gaussian distributions reasonably represent the numerically simulated data, where R^2 values for these curve-fits are between 0.97 and 0.99

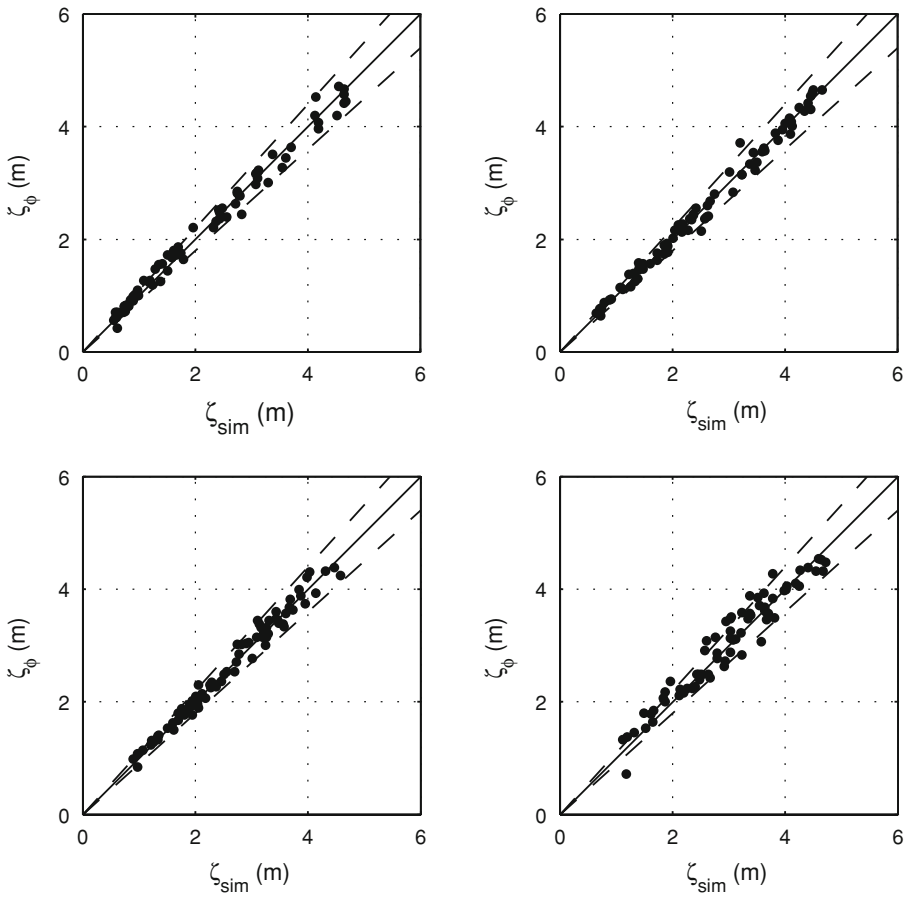

Fig. 11 Predicted surge using curve-fitted surge response function, based on all four tracks, versus numerically simulated surge at Locations 1 (*top left*), 2 (*top right*), 3 (*bottom left*), and 4 (*bottom right*). Solid line indicates an exact match while dashed lines indicate ±10% about an exact match

at Locations 1 through 3 and 0.91 at Location 4. To test the skill of Φ for surge response estimation, we first used the curve-fitted function of Eq. 7 was used to estimate surge (ζ_Φ) based on the suite of 75 meteorological input parameter combinations, namely $R_p - c_p - x_o$ sets. These estimated surges were then compared with the numerically simulated surges (ζ_{sim}, Fig. 11). At all locations, the mean ($\zeta_\Phi - \zeta_{sim}$) errors are between 0 and +4 cm (Table 1) and can be considered negligible, given expected error in the surge simulations on the order of 20–30 cm. At Locations 1 through 3, root-mean-square (RMS) error in ζ_Φ is between 13 and 14 cm while RMS error at Location 4 is somewhat larger, 24 cm. The RMS errors in ζ_Φ are the same order of magnitude as the expected simulation error (typically 20–30 cm) and for risk-analysis can be accounted for through an uncertainty term.

3.2.1 Limited number of discrete storm tracks

Next, the case where simulated surge data are available for a limited number of tracks was examined by considering an increase in track spacing from 30 km (0.25°) to 60 km (0.50°)

Table 1 Error statistics for surge prediction using surge response functions

Track spacing (km [°])	Tracks included	Statistics for storms within bounds of included data for all locations (range)			Statistics for all 75 storms for all locations (range)		
		Mean error [% mean error] (cm)[a]	RMS error [% RMS error] (cm)[a]	R^2	Mean error (cm)[a]	RMS error (cm)[a]	R^2
30 [0.25]	A, B, C, D (baseline)	+2 [+1.2] (0 to +4)	16 [7.3] (13 to 24)	0.97 (0.94–0.99)	All storms within data bounds		
60 [0.50]	A, C	−2 [−5.1] (−9 to +4)	15 [5.7] (10–19)	0.98 (0.97–0.99)	−4 (−15 to +6)	28 (10 to 43)	0.94 (0.91 to 0.99)
	B, D	+4 [+2.2] (+0 to +8)	19 [7.5] (11–25)	0.96 (0.92–0.98)	+12 (0 to +30)	43 (19 to 106[b])	0.89 (0.70[b] −0.97)
90 [0.75]	A, D	−6 [−1.0] (−16 to +9)	22 [7.7] (15–30)	0.96 (0.94–0.99)	All storms within data bounds		
90 [0.75]	A, D when $c_p = 900$ and 960 mb only	−6 [−2.7] (−17 to +10)	23 [8.4] (16–32)	0.97(0.94–0.99)	All storms within data bounds		
Spatial interpolation using Locations 1 and 4 to predict Locations 2 and 3 (Loc 2, Loc 3)		+20 [5.5], +23 [7.4]	27 [7.6], 32 [10.2]	0.95, 0.92	+25, +2	61, 71	0.83, 0.76

[a] Data in parenthesis () give range of error at all four locations, in cm

[b] Larger error values are associated with those locations without data coverage for $x_2' > 0$

Fig. 12 Dimensionless surge response functions using simulated storm surge for the 60-km spacing cases of Tracks A and C only (top pane) and Tracks B and D only (bottom pane). Within each pane are Locations 1 (*top left*), 2 (*top right*), 3 (*bottom left*), and 4 (*bottom right*). Solid line shows 3-term Gaussian fit to data ▶

and 90 km (0.75°). Figures 12 and 13 show the simulation data points and corresponding Φ curve-fit for these more sparsely spaced track conditions while Figs. 14 and 15 show the predicted ζ_Φ versus ζ_{sim} for these cases. For the 60-km spacing case using Tracks A and C (Figs. 12 and 14, top panes), at Locations 1 through 4 the simulated data points span a range of x_2' from negative, to near-zero, to positive, thereby providing sufficient information for curve-fitting, particularly in the region of highest surge potential $\left(x_2' \approx 0\right)$. The resulting ζ_Φ predictions yield error magnitudes (average mean error = −4 cm and average RMS error = 28 cm, Table 1) similar in order-of-magnitude to those characterizing the predictions with the full four-track suite of simulated data. Similar magnitudes of error are also observed for the ζ_Φ predictions for the 60-km Tracks B and C case at Locations 2 through 4 (Figs. 12 and 14, bottom panes, and Table 1). However, at Location 1 for the Tracks B and C cases more error is introduced, particularly for the more extreme surge levels. This is primarily a consequence of no data coverage about the peak of the surge response function distribution $\left(x_2' \approx 0\right)$ and secondarily a consequence of no data coverage when $\left(x_2' < 0\right)$. In other words, the response function is not as well represented when data are not available for storms tracking to the right of the location of interest, in the range $x_2' \geq 0$. However, it is anticipated, based on the results for the Tracks A and C case, that the addition of simulations along a track 60 km to the south of Location 1 should provide sufficient information for response function development.

For the case when two tracks spaced 90 km apart (Tracks A and D) are used to develop Φ and predict ζ_Φ (Figs. 13 and 15), at Locations 1 through 3 values of x_2' span a range from negative to positive, including simulated data near $x_2' = 0$. At these locations, the resulting ζ_Φ predictions yield error magnitudes (average mean error = −6 cm and average RMS error = 22 cm, Table 1) similar in order-of-magnitude to those characterizing the predictions with tracks spaced every 30 or 60 km. At Location 4, while values of x_2' do span from negative to positive there is a noticeable gap in x_2' coverage near the peak of the Φ distribution $\left(x_2' \approx 0\right)$. Unlike at Location 1 for the 60-km Tracks B and D case, here there are simulated data points available to either side of $x_2' = 0$. By estimating the peak value of ζ' at $x_2' = 0$, a Gaussian fit in the form of Eq. 7 which has a peak near $x_2' = 0$ may be developed. Here, this false data point was represented by the average between the linearly extrapolated values of ζ' using the available simulated ζ' values in the regimes $x_2' < 0$ and $x_2' > 0$. The resulting Φ curve-fits shown in Fig. 13 (bottom right), and Fig. 14 (bottom right) indicate that this extrapolation procedure shows promise for response function development in locations where data for most extreme surge values are not available. At Location 4, this modified curve-fit for Φ results in a surge prediction with mean and RMS errors of −16 and 30 cm.

The above analysis indicates that a numerical simulation set with tracks spaced at least 90 km apart, possibly more, is sufficient for predicting surge response at any open coast location between tracks. With track spacing increased from 30 km (0.25°) to 90 km (0.75°), the number of numerical simulations are reduced by half, from 75 to 38.

3.2.2 Limited number of discrete storm intensities

In this section, the accuracy of Φ and related surge predictions (ζ_Φ) was evaluated when the number of unique storms on each track is also limited. Since it is desirable to consider a

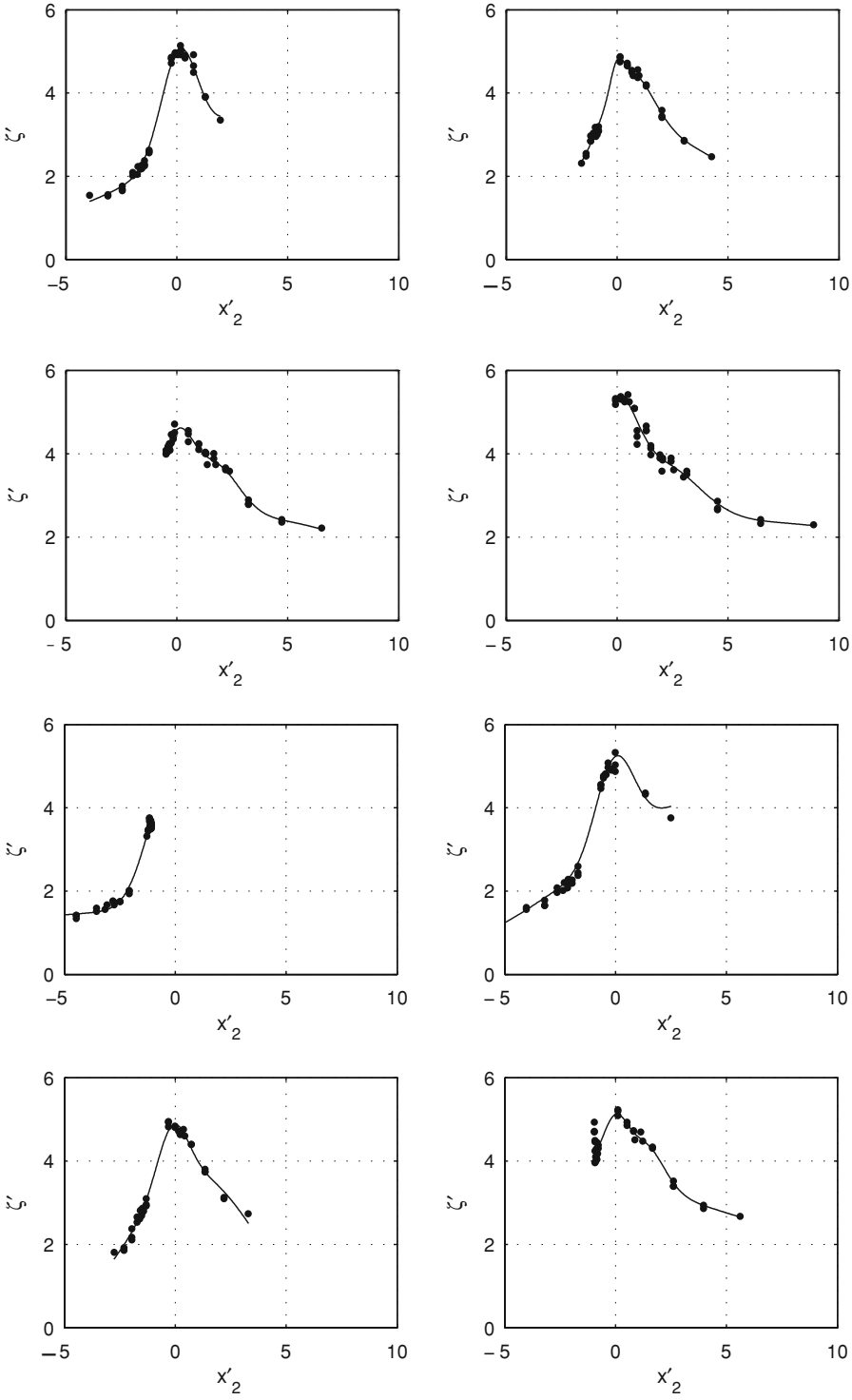
ζ′
x′2
0
2
4
6
−5
0
5
10

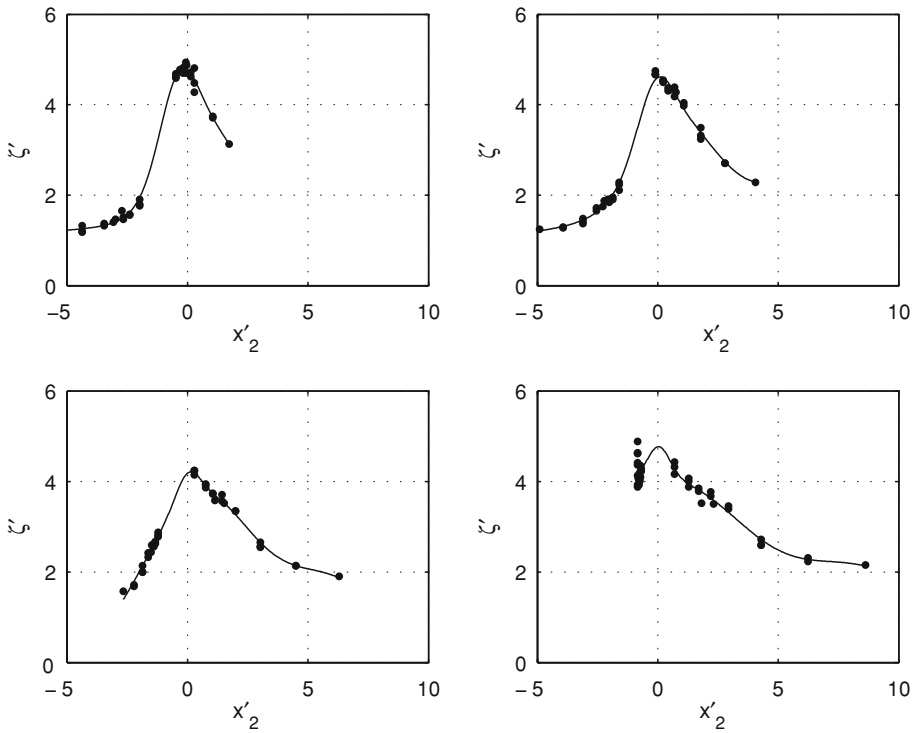

Fig. 13 Dimensionless surge response functions using simulated storm surge for Tracks A and D only (90-km spacing). Within each pane are Locations 1 (*top left*), 2 (*top right*), 3 (*bottom left*), and 4 (*bottom right*). Solid line shows 3-term Gaussian fit to data

range of x_2' values (or R_p values), here the along-track storm set is reduced by considering a limited set of c_p. Choosing the subset of simulated storms on Tracks A and D when $c_p = 900$ or 960 mb results in the response function and surge predictions shown in Figs. 16 and 17. It is worth noting that while the combined storm set on Tracks A and D was reduced by more than half, from 38 storms (Figs. 13 and 15) to 18 storms (Figs. 16 and 17), the response function and prediction accuracy (Table 1) is remarkably similar between these cases. This analysis shows that numerical simulations can be optimized by limiting both the number of tracks and the number of intensity scenarios considered. Here, the total realized computational reduction was 75%.

3.2.3 Limited spatial information

For many engineering investigations, budget and time constraints limit surge data analysis to interrogation of historical water level gauge measurements or high water marks. Given

Fig. 14 Predicted surge using curve-fitted surge response function, based on Tracks A and C only (top pane) and Tracks B and D (bottom pane), versus numerically simulated surge at Locations 1 (*top left*), 2 (*top right*), 3 (*bottom left*), and 4 (*bottom right*). Solid line indicates an exact match, dashed lines indicate ±10% about an exact match, and hollow circles indicate prediction is extrapolated beyond the bounds of the surge response function ▶

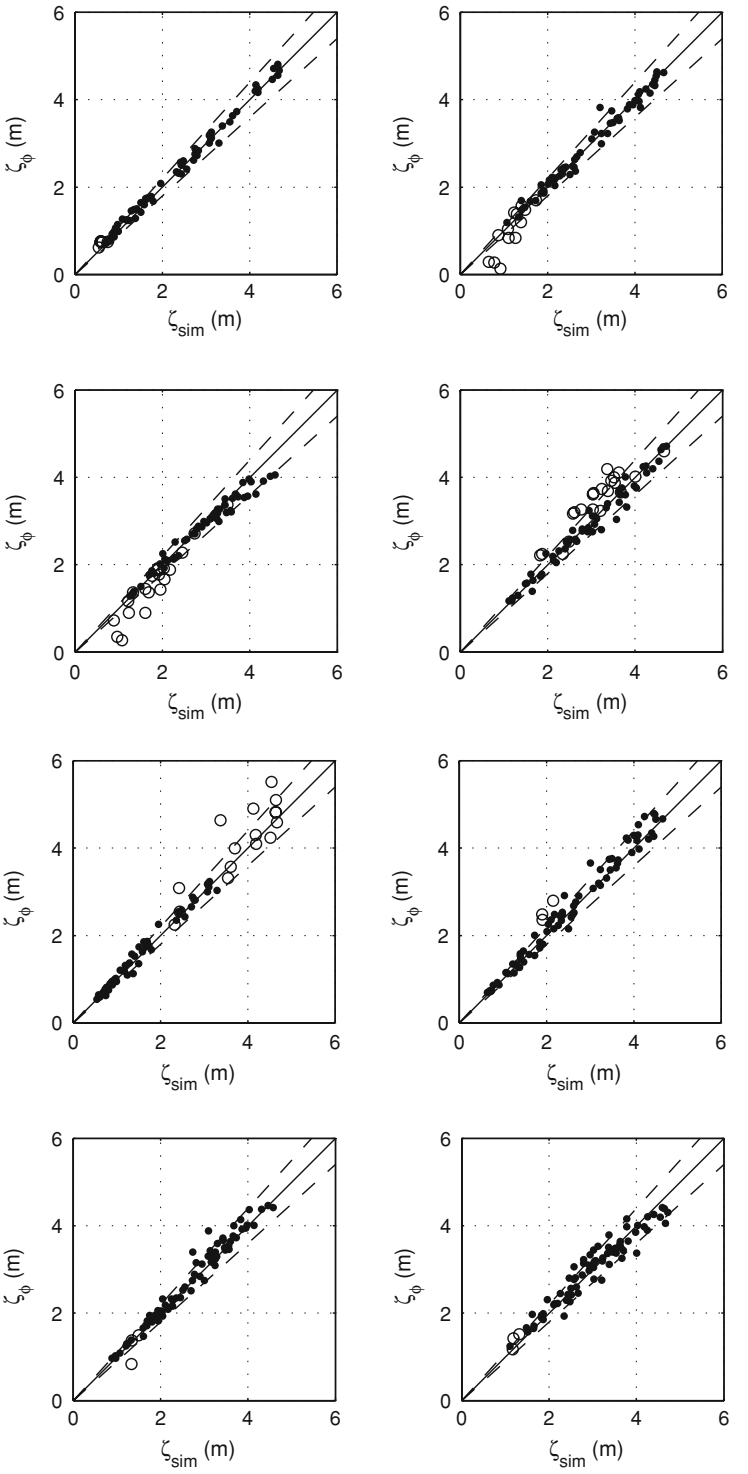
ζ_ϕ (m)
ζ_{sim} (m)
0
2
4
6

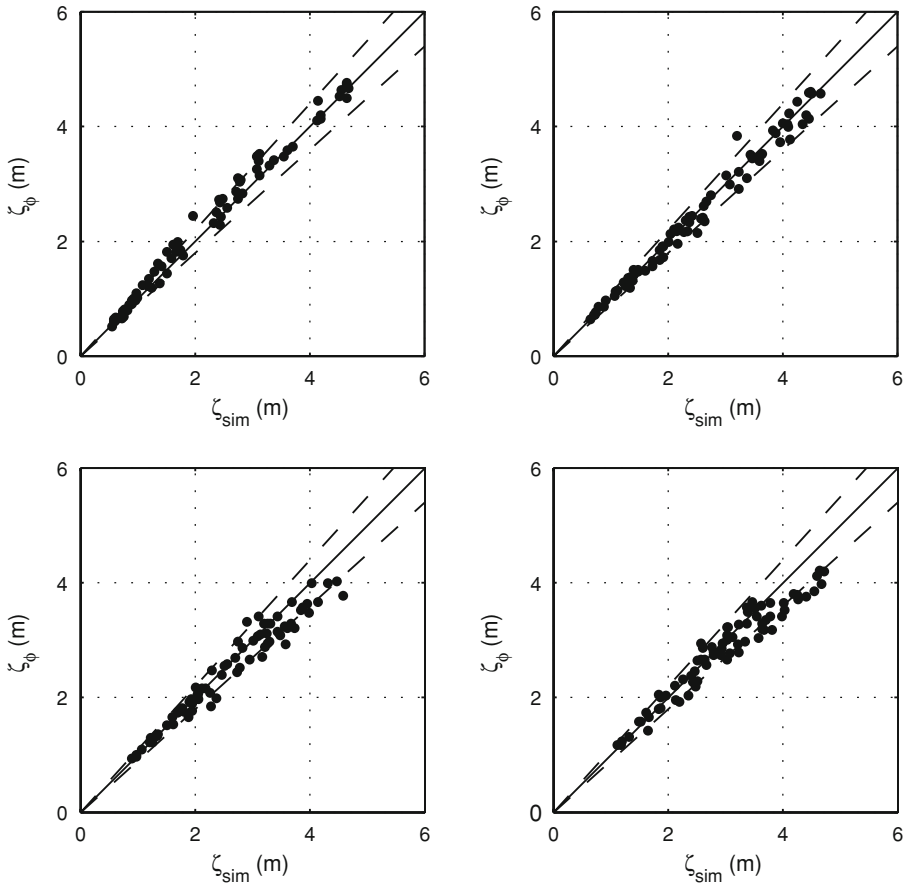

Fig. 15 Predicted surge using curve-fitted surge response function, based on Tracks A and D only, versus numerically simulated surge at Locations 1 (*top left*), 2 (*top right*), 3 (*bottom left*), and 4 (*bottom right*). Solid line indicates an exact match while dashed lines indicate ±10% about an exact match

the slowly varying changes in Φ with along-coast location, the accuracy and viability of using weighted-averaging to interpolate response functions along the coast was evaluated. Starting with the Track A and Track D functions for the full set of simulated storms the response functions at Locations 2 and 3 were estimated by taking an alongshore-distance weighted average between the response functions at Locations 1 and 4, within the region of x_2' overlap. The resulting surge predictions at Locations 2 and 3, within the range of $\Phi(x_2')$ computed explicitly shows good agreement with the simulated surges at both locations particularly for larger surge events (Fig. 18). Mean and RMS errors for this distance-weighted interpolation between gauges spaced 90 km apart is within 23 and 32 cm, respectively (Table 1). The surge predictions do, however, exhibit more scatter when determined by straight extrapolation of the surge response function. This evaluation indicates that the surge response function approach can expand the quantitative use of historical data to include locations for which no measurements are available.

The analysis described above demonstrates that a small sample of hurricane surges may be used to define the surge response over a wide range of meteorological and geographic

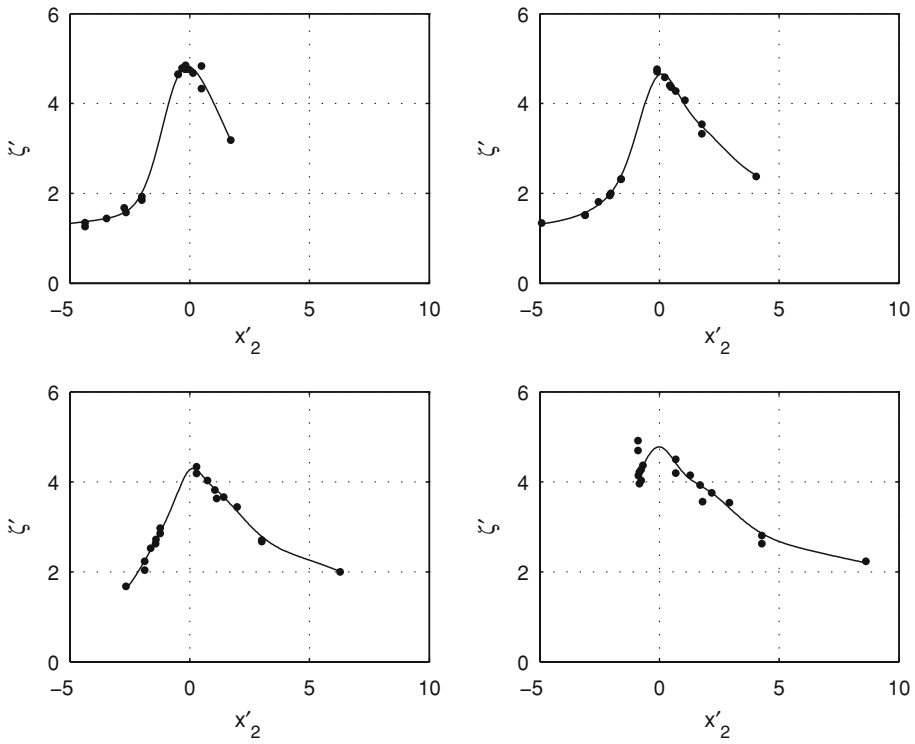

Fig. 16 Dimensionless surge response functions using simulated storm surge for Tracks A and D with $c_p = 900$ or 960 mb only (90-km spacing). Within each pane are Locations 1 (*top left*), 2 (*top right*), 3 (*bottom left*), and 4 (*bottom right*). Solid line shows 3-term Gaussian fit to data

conditions. Such a method may be used to identify storm conditions to be combined with an optimal sampling method for hazard risk assessment (Neidoroda et al. in review).

4 Summary and conclusions

The surge response surface approach to coastal storm surge statistics with the JPM-OS method allows the use of a continuous probability density function. Resio et al. (2009) showed that such an approach can provide a more effective risk assessment for extreme events. Here, the authors first showed that surge response surfaces exhibit continuous behavior with respect to storm intensity, storm size, and storm track over a large coastal area. Secondly, it was demonstrated that a dimensionless surge response function exists and can reasonably be described in terms of physical scaling laws relating the location of peak alongshore surge to storm size and the surge magnitude to storm intensity. Finally, the numerically simulated data were decimated to demonstrate the use of the developed scaling laws to estimate surge response functions with a high degree of accuracy.

The dimensionless surge response function and interpolation scheme introduced here can readily be applied in open coastal areas. Because this response function approach produces reliable surge estimates, particularly for the high surge levels important to extreme-value statistics, this approach has the potential to reduce numerical simulation

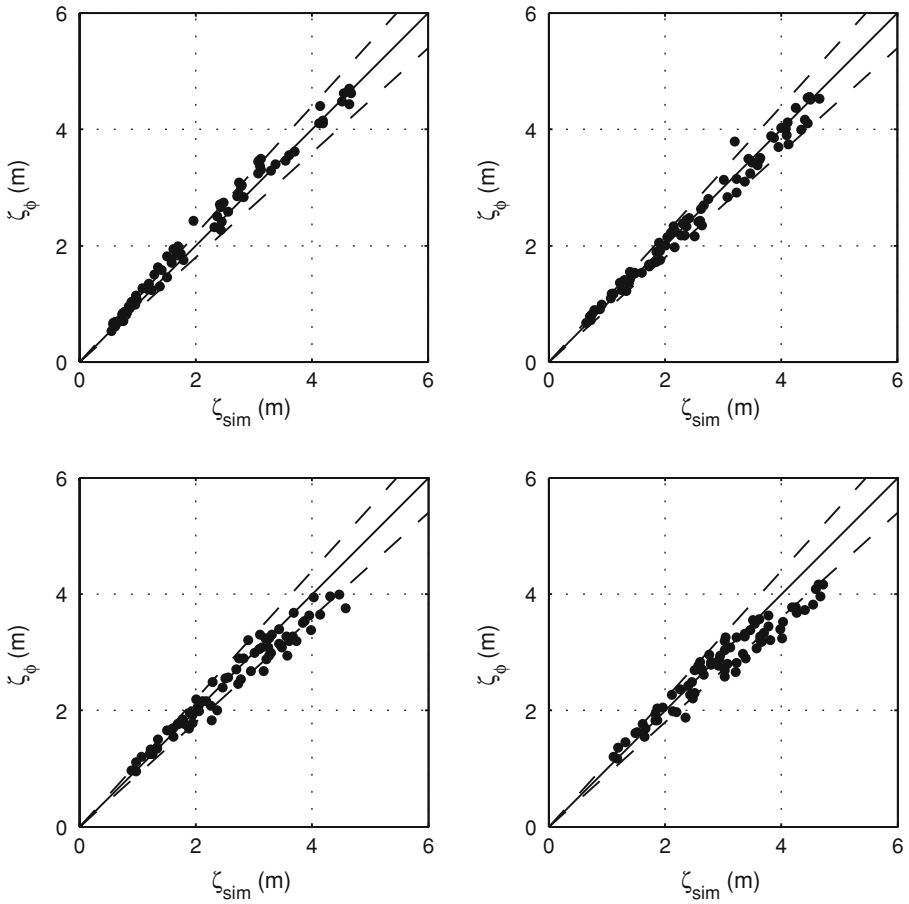

Fig. 17 Predicted surge using curve-fitted surge response function, based on Tracks A and D with $c_p = 900$ or 960 mb only, versus numerically simulated surge at Locations 1 (*top left*), 2 (*top right*), 3 (*bottom left*), and 4 (*bottom right*). Solid line indicates an exact match while dashed lines indicate $\pm 10\%$ about an exact match

requirements by at least 75% for coastal hazard assessment studies. Such computational time savings will lead to significant project time and cost savings. Similarly, this dimensionless response function approach shows promise for historical data interpretation. Limited surge level observations at discrete locations along with information on intensity, size, and track of those hurricanes captured in the surge observation record may be analyzed in the context of these response functions in order to estimate surge levels for alternate events at the measurement location, or at other locations along the same stretch of coast.

Finally, for more comprehensive application in hurricane surge studies, the response functions developed here should be expanded to include the impacts of other physical processes such as storm angle of approach and forward speed, wave setup, inland runoff, and locally generated wind setup. It is expected that a more generalized dimensionless response function exists and can be described in a similar manner as that presented here.

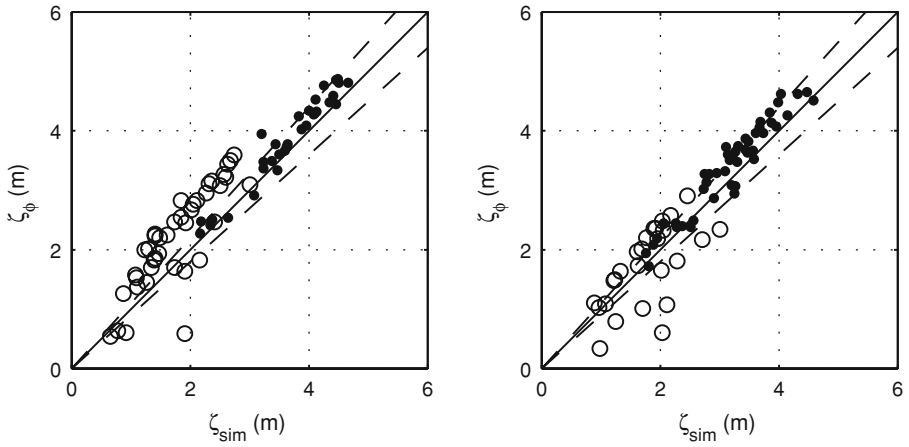

Fig. 18 Predicted surge at Locations 2 (*left*) and 3 (*right*) using a weighted-average of curve-fitted surge response functions at Locations 1 and 2 (see Fig. 10). Solid line indicates an exact match, dashed lines indicate ±10% about an exact match, and hollow circles indicate prediction is extrapolated beyond the bounds of the interpolated surge response function

Acknowledgments The research presented herein was funded by the U.S. Army Engineer Research and Development Center and in part by a Grant/Cooperative Agreement from the National Oceanic and Atmospheric Administration. The views expressed herein are those of the authors and do not necessarily reflect views of NOAA or any of its subagencies. The use of trade names does not constitute an endorsement in the use of these products by the U.S. Government.

References

Dorst N (2007) What is the average forward speed of a hurricane? In Hurricane Research Division Frequently Asked Questions. National Oceanic and Atmospheric Administration. http://www.aoml.noaa.gov/hrd/tcfaq/G16.html

Holland GJ (1980) An analytic model of the wind and pressure profiles in hurricanes. Mon Weather Rev 108:1212–1218. doi:10.1175/1520-0493(1980)108<1212:AAMOTW>2.0.CO;2

Irish JL, Resio DT, Ratcliff JJ (2008) The influence of storm size on hurricane surge. J Phys Oceanogr (online) doi:10.1175/2008JPO3727.1

Niedoroda AW, Resio DT, Toro G, Divoky D, Reed C (in review) Emerging methods for evaluation of the coastal hurricane storm surge hazard. *Ocean Engineering*

Resio DT, Irish JL, Cialone MA (2009) A surge response function approach to coastal hazard assessment – part 1: basic concepts. Nat Hazards. doi:10.1007/s11069-009-9379-y

Thompson EF, Cardone VJ (1996) Practical modeling of hurricane surface wind fields. J Waterw Port C ASCE 122(4):195–205

U.S. Army Corps of Engineers (2006a) Performance evaluation of the New Orleans and southeast Louisiana hurricane protection system draft final report of the Interagency Performance Evaluation Task Force. U.S. Army Corps of Engineers Report, 259 pp

U.S. Army Corps of Engineers (2006b) Louisiana Coastal Protection and Restoration (LACPR) preliminary technical report—appendix B—history of hurricane occurrences. U.S. Army Corps of Engineers New Orleans District Report

Westerink JJ, Luettich RA, Baptista AM, Scheffner NW, Farrar P (1992) Tide and storm surge predictions using finite element model. J Hydr Eng 118(10):1373–1390. doi:10.1061/(ASCE)0733-9429(1992)118:10(1373)

Westerink JJ, Luettich RA, Feyen JC, Atkinson C, Dawson MD, Powell JP, Roberts HJ, Kubatko EJ, Pourtaheri H (2007) A basin to channel scale unstructured grid hurricane storm surge model as implemented for southern Louisiana. Mon Weather Rev 136:833–864